IOPscience iopscience.iop.org

Home Search Collections Journals About Contact us My IOPscience

Two-wavelength full-field heterodyne interferometric profilometry

This content has been downloaded from IOPscience. Please scroll down to see the full text.

2009 Meas. Sci. Technol. 20 025307

(http://iopscience.iop.org/0957-0233/20/2/025307)

View the table of contents for this issue, or go to the journal homepage for more

Download details:

IP Address: 140.113.38.11

This content was downloaded on 25/04/2014 at 11:34

Please note that terms and conditions apply.

IOP Publishing Measurement Science and Technology

Meas. Sci. Technol. **20** (2009) 025307 (5pp) doi:10.1088/0957-0233/20/2/025307

Two-wavelength full-field heterodyne interferometric profilometry

Hung-Chih Hsieh, Yen-Liang Chen, Zhi-Chen Jian, Wang-Tsung Wu and Der-Chin Su[1]

Department of Photonics and Institute of Electro-Optical Engineering, National Chiao-Tung University, 1001 Ta-Hsueh Road, Hsinchu 30050, Taiwan, Republic of China

E-mail: t7503@faculty.nctu.edu.tw

Received 18 August 2008, in final form 10 December 2008
Published 13 January 2009
Online at stacks.iop.org/MST/20/025307

Abstract

An alternative full-field interferometric profilometry is proposed by combining two-wavelength interferometry and heterodyne interferometry. A collimated heterodyne light is introduced into a modified Twyman–Green interferometer, the full-field interference signals are taken by a fast CMOS camera. The sampled intensities recorded by each pixel are fitted to derive a sinusoidal signal with the least-square sine wave fitting algorithm, and its phase can be obtained. Comparing the phase of the reference point, the relative phase of the pixel can be calculated. Next, the same measurement is made again at a different wavelength. The relative phase with respect to the effective wavelength can be calculated and the profile of the tested sample can be derived with the two-wavelength interferometric technique. Its validity is demonstrated. It has merits of both two-wavelength interferometry and heterodyne interferometry.

Keywords: two-wavelength interferometry, heterodyne interferometry, full-field measurement, profilometry, sine wave fitting algorithm

1. Introduction

High-precision and time-saving methods for measuring surface profiles are required in many fields of science and industry. Interferometric profilers using monochromatic light offer excellent vertical resolution, but a serious limitation to their use is 2π phase ambiguities that arise if the measurement range involves a change in the optical path difference greater than a wavelength. Phase unwrapping techniques can be used only with smooth continuous surfaces and break down where the test surface exhibits a sharp step or a discontinuity. To overcome these drawbacks, several non-contact and non-destructive optical methods [1–12] have been proposed and they have good measurement results. In this paper, an alternative full-field interferometric profilometry is proposed by combining two-wavelength interferometry [13, 14] and heterodyne interferometry [15, 16]. The light beam coming from a heterodyne light source is collimated and enters a modified Twyman–Green interferometer, the full-field interference signals are taken by a fast CMOS camera. Each pixel records a series of sampled points of its corresponding sinusoidal signal. Based on a least-square sine wave fitting algorithm [17, 18], an optimal fitted sine wave curve and the associated phase can be obtained. Compared with the phase of the reference point, the relative phase of the pixel can be calculated. Next, the same measurement is made again at a different wavelength, and the relative phase with respect to the effective wavelength can be calculated with the two-wavelength interferometric technique. The processes are applied to other pixels; their relative phases can be estimated similarly. Consequently, the profile of the tested sample can be derived. The validity of this method is demonstrated. It has merits of both two-wavelength interferometry and heterodyne interferometry.

[1] Author to whom any correspondence should be addressed.

2. Principle

2.1. The optical configuration and the interference intensity

The optical configuration of this method is shown in figure 1. A heterodyne light source [14] is used in this method, and it has

 © 2009 IOP Publishing Ltd Printed in the UK

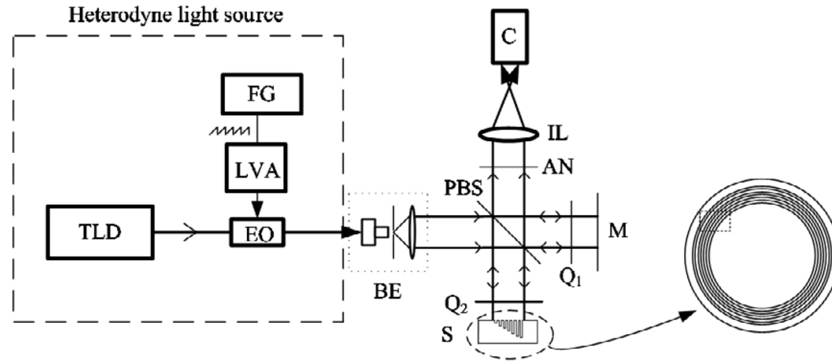

Figure 1. The optical configuration of this method. TLD: tunable laser diode; EO: electro-optic modulator; FG: function generator; LVA: linear voltage amplifier; BE: beam expander; PBS: polarizing beam-splitter; Q1, Q2: quarter-wave plates; M: mirror; S: sample; AN: analyzer; IL: imaging lens; C: CMOS camera.

a tunable laser diode (TLD), an electro-optic modulator (EO), a function generator (FG) and a linear voltage amplifier (LVA). For convenience, the z-axis is chosen along the propagation direction and the y-axis is along the vertical direction. A light beam with frequency f_0 coming from the light source [19] is the combined vector components of the s- and p-polarizations and has a frequency difference f between them, then its Jones vector can be written as

$$E = \frac{1}{\sqrt{2}}\begin{pmatrix} e^{i\pi f t} \\ e^{-i\pi f t}\end{pmatrix} e^{i2\pi f_0 t}. \quad (1)$$

The light beam passing through a beam expander (BE) enters a modified Twyman–Green interferometer, which consists of a polarization beam splitter (PBS), two quarter-wave plates (Q_1, Q_2) with the fast axes at 45° with respect to the x-axis, a reference mirror (M), a tested sample (S), an analyzer (AN) with the transmission axis at 45° with respect to the x-axis, an imaging lens (L) and a CMOS camera (C). In the interferometer, the collimated light beam is divided into two beams by the PBS; their paths are PBS → Q_2 → S → Q_2 → PBS → AN → IL → C (the test beam) and PBS → Q_1 → M → Q_1 → PBS → AN → IL → C (the reference beam), respectively. Consequently, their amplitudes E_t and E_r can be expressed as

$$\begin{aligned} E_t &= \mathrm{AN}(45^\circ)\cdot R_{\mathrm{PBS}}\cdot Q_2(-45^\circ)\cdot S\cdot Q_2(45^\circ)\cdot T_{\mathrm{PBS}}\cdot E \\ &= \frac{1}{2}\begin{pmatrix}1 & 1\\ 1 & 1\end{pmatrix}\begin{pmatrix}1 & 0\\ 0 & 0\end{pmatrix}\frac{1}{\sqrt{2}}\begin{pmatrix}1 & i\\ i & 1\end{pmatrix} \\ &\quad\times\begin{pmatrix}-r_s e^{i\frac{4\pi\Delta d(x,y)}{\lambda}} & 0\\ 0 & r_s e^{i\frac{4\pi\Delta d(x,y)}{\lambda}}\end{pmatrix}\frac{1}{\sqrt{2}}\begin{pmatrix}1 & -i\\ -i & 1\end{pmatrix} \\ &\quad\times\begin{pmatrix}0 & 0\\ 0 & 1\end{pmatrix}\frac{1}{\sqrt{2}}\begin{pmatrix}e^{i\pi f t}\\ e^{-i\pi f t}\end{pmatrix}e^{i2\pi f_0 t} \\ &= \frac{ir_s}{4\sqrt{2}}\begin{pmatrix}1\\ 1\end{pmatrix}e^{i\left(\pi f t+\frac{4\pi\Delta d(x,y)}{\lambda}\right)}e^{i2\pi f_0 t}, \end{aligned} \quad (2)$$

and

$$\begin{aligned} E_r &= \mathrm{AN}(45^\circ)\cdot T_{\mathrm{PBS}}\cdot Q_1(-45^\circ)\cdot M\cdot Q_1(45^\circ)\cdot R_{\mathrm{PBS}}\cdot E \\ &= \frac{1}{2}\begin{pmatrix}1 & 1\\ 1 & 1\end{pmatrix}\begin{pmatrix}1 & 0\\ 0 & 0\end{pmatrix}\frac{1}{\sqrt{2}}\begin{pmatrix}1 & i\\ i & 1\end{pmatrix}\begin{pmatrix}-r_m & 0\\ 0 & r_m\end{pmatrix} \\ &\quad\times\frac{1}{\sqrt{2}}\begin{pmatrix}1 & -i\\ -i & 1\end{pmatrix}\begin{pmatrix}0 & 0\\ 0 & 1\end{pmatrix}\frac{1}{\sqrt{2}}\begin{pmatrix}e^{i\pi f t}\\ e^{-i\pi f t}\end{pmatrix}e^{i2\pi f_0 t} \\ &= -\frac{ir_m}{4\sqrt{2}}\begin{pmatrix}1\\ 1\end{pmatrix}e^{-i\pi f t}e^{i2\pi f_0 t}, \end{aligned} \quad (3)$$

where T_{PBS} and R_{PBS} are the transmission matrix and the reflection matrix of the PBS, $2\Delta d(x, y)$ is the optical path difference between these two beams; r_m and r_s are the amplitude reflection coefficients of the M and the S; λ is the wavelength of the light source. So, the interference intensity detected by the C is

$$I = |E_t + E_r|^2 = I_0 + \gamma\cos(2\pi f t + \phi), \quad (4)$$

where $I_0 = \frac{1}{16}\left(r_s^2 + r_m^2\right)$ and $\gamma = -\frac{r_s r_m}{8}$. The phase term $e^{i2\pi f_0 t}$ is cancelled out during the intensity calculations. ϕ is the phase difference between them and it can be expressed as

$$\phi(x, y) = \frac{4\pi\Delta d(x, y)}{\lambda} = \phi_1(x_r, y_r) + \phi_2(x, y). \quad (5)$$

Here $\phi_1(x_r, y_r)$ is the phase difference at the reference point (x_r, y_r) on the M and it depends on the optical setup. On the other hand, $\phi_2(x, y)$ is the relative phase difference which will be measured and can be expressed as

$$\phi_2(x, y) = \frac{4\pi h(x, y)}{\lambda}, \quad (6)$$

where $h(x, y)$ is the height distribution with respect to (x_r, y_r). So, we have $\phi_2(x_r, y_r) = 0$, that is $\phi_1(x_r, y_r) = \phi(x_r, y_r)$ in our method.

2.2. *Phase estimation*

A CMOS camera with frame frequency f_s and frame exposure time Δt is used to take n frames in a phase measurement time T, so every pixel records a series of n interference intensities which are the sampled points of a sinusoidal signal, as shown in figure 2. If n interference intensities recorded by any pixel at time $t_1, t_2, \ldots, t_n$ are $I_1, I_2, \ldots, I_n$, respectively, then we have

$$\begin{aligned} I_k &= \frac{1}{\Delta t}\int_{(k-1)/f_s}^{[(k-1)/f_s]+\Delta t} I_0(1+\gamma\cos(2\pi f t+\phi))\,dt \\ &= I_0\left\{1+\gamma'\cos\left(\frac{2\pi f(k-1)}{f_s}+\pi f\Delta t+\phi\right)\right\}, \end{aligned} \quad (7)$$

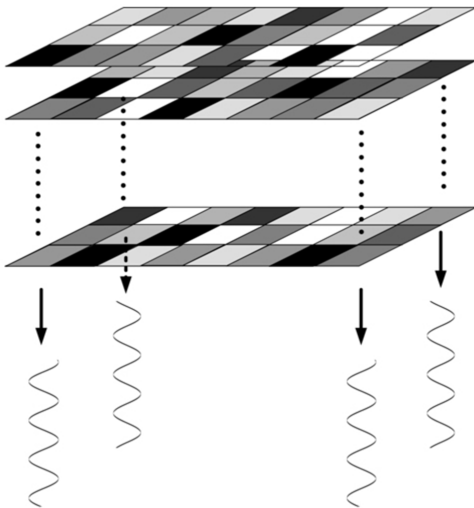

Figure 2. A series of n interference intensities recorded by every pixel.

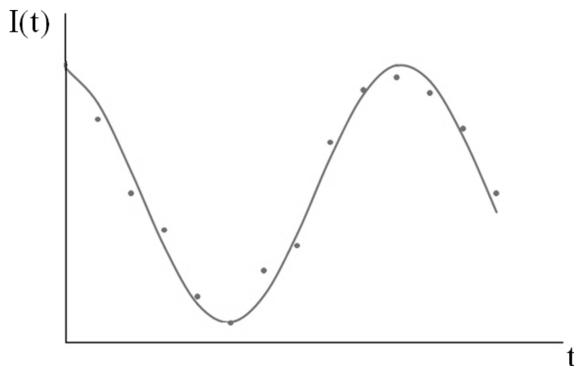

Figure 3. The sampled points and the associated fitted sinusoidal curve.

(This figure is in colour only in the electronic version)

where $\gamma' = \gamma \mathrm{sinc}(f\Delta t)$. Next, I_k will be quantized in gray-level units and it can be modified as

$$I_{kg} = \mathrm{Round}\left[\frac{1 + \mathrm{sinc}(f\Delta t)\cos\left(\frac{2\pi f(k-1)}{f_s} + \phi'\right)}{2I_0}g\right], \quad (8)$$

where Round $[x]$ is a mathematical operator to round the number x to an integer; g is the gray level of the CMOS camera; ϕ' is the phase of the sampled interference signal and it has

$$\phi' = \pi f\Delta t + \phi. \quad (9)$$

The sampled data of I_{kg} are depicted as a series of dots which can be further fitted to derive an optimal sine curve, as shown in figure 3. The equation of the fitted sine curve has the form of

$$I'(t_k) = A_0\cos(2\pi f t_k) + B_0\sin(2\pi f t_k) + C_0$$
$$= \sqrt{A_0^2 + B_0^2}\cos(2\pi f t_k + \phi'), \quad (10)$$

where

$$\phi' = \tan^{-1}\left(-\frac{B_0}{A_0}\right) \quad (11)$$

A_0, B_0 and C_0 are constants. According to the least-square method [17], they can be obtained by minimizing the sum of the quadratic errors

$$S = \sum_{k=1}^{n}[I_{kg} - I'(t_k)]^2. \quad (12)$$

Partially differentiating equation (12) with respect to A_0, B_0 and C_0 and then equating the derivatives to zero gives a linear system of three equations

$$D_0 x = y, \quad (13)$$

where

$$D_0 = \begin{pmatrix} \sum_{k=1}^{n}\cos(2\pi f t_k) & \sum_{k=1}^{n}\cos^2(2\pi f t_k) & \sum_{k=1}^{n}\cos(2\pi f t_k)\sin(2\pi f t_k) \\ \sum_{k=1}^{n}\sin(2\pi f t_k) & \sum_{k=1}^{n}\cos(2\pi f t_k)\sin(2\pi f t_k) & \sum_{k=1}^{n}\sin^2(2\pi f t_k) \\ n & \sum_{k=1}^{n}\cos(2\pi f t_k) & \sum_{k=1}^{n}\sin(2\pi f t_k) \end{pmatrix};$$

$$x = \begin{pmatrix} A_0 \\ B_0 \\ C_0 \end{pmatrix}; \quad \text{and} \quad y = \begin{pmatrix} \sum_{k=1}^{n} I_{kg}\cos(2\pi f t_k) \\ \sum_{k=1}^{n} I_{kg}\sin(2\pi f t_k) \\ \sum_{k=1}^{n} I_{kg} \end{pmatrix} \quad (14)$$

Consequently, we have

$$x = D_0^{-1}y, \quad (15)$$

where D_0^{-1} means the inverse matrix of D_0. From equation (15), A_0 and B_0 can be calculated. They are substituted into equation (11) to obtain ϕ'. Finally, the measured phase ϕ can be calculated from equation (9). If these processes are applied to other pixels, then their phases can be obtained similarly. By substituting the data of $\phi(x, y)$ into equation (5), $\phi_2(x, y)$ can be calculated.

2.3. *The two-wavelength interferometric method [3]*

To avoid the phase discontinuity, the two-wavelength interferometric method is used. If the data of $\phi_2(x, y)$ are $\phi_a(x, y)$ and $\phi_b(x, y)$ at two wavelengths λ_a and λ_b, respectively, then we have

$$h(x, y) = \frac{\phi_b(x, y) - \phi_a(x, y)}{4\pi}\Lambda, \quad (16)$$

where Λ is the effective wavelength and it can be expressed as

$$\Lambda = \frac{\lambda_a\lambda_b}{|\lambda_a - \lambda_b|}. \quad (17)$$

If λ_a and λ_b are very close in value, then the effective wavelength Λ will be relatively large in comparison to either of them. Furthermore, the unambiguity range can be increased accordingly. Consequently, from equations (16) and (17), it is obvious that $h(x, y)$ can be calculated with the specified data of $\phi_a(x, y)$, $\phi_b(x, y)$ and Λ.

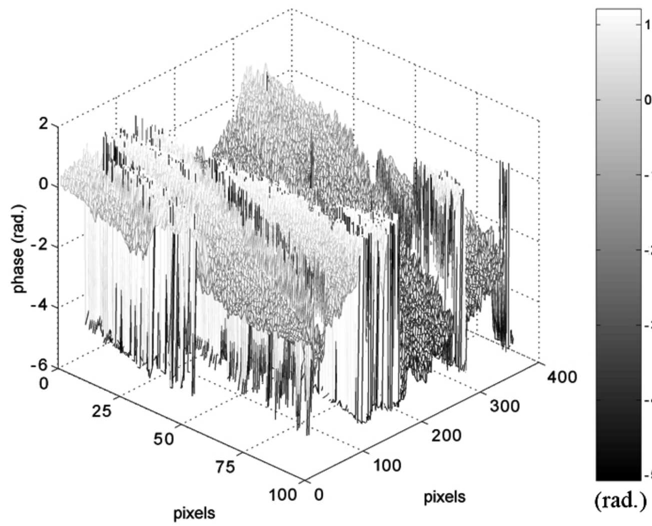

Figure 4. The two-dimensional phase distribution of $\phi_2(x, y)$ at $\lambda_a = 633.00$ nm.

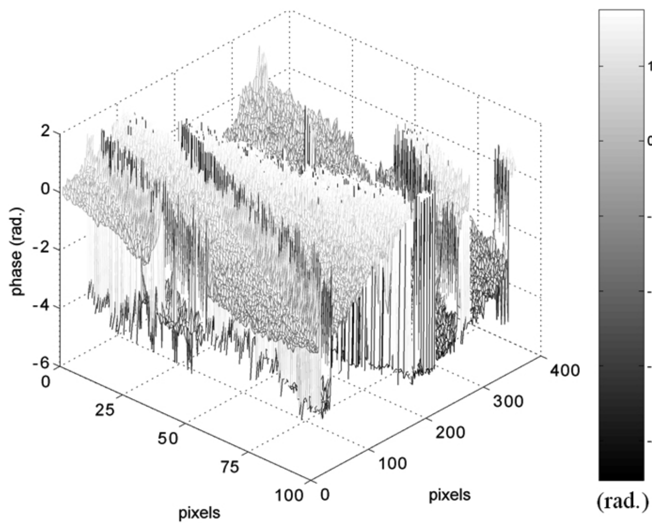

Figure 5. The two-dimensional phase distribution of $\phi_2(x, y)$ at $\lambda_b = 635.00$ nm.

3. Experiments and results

In order to show the feasibility, we tested a sample with several concentric grooves as shown in the right part of figure 1. For convenience, only a 10 mm × 3 mm rectangular dashed part shown in the figure was tested. A CMOS camera (Baslar/A504 k) with 350 × 100 pixels and 8 bit gray levels was used under the conditions $f = 30$ Hz, $f_s = 450$ fps, $\Delta t = 1$ ms and $T = 1$ s. A tunable laser (New Focus/Model 6304) with 0.02 nm wavelength resolution was introduced at $\lambda_a = 633.00$ nm and $\lambda_b = 635.00$ nm. The conjugate point of the pixel (10, 10) was chosen as the reference point, and the measured results of $\phi_a(x, y)$ and $\phi_b(x, y)$ are depicted in figures 4 and 5, respectively. The data of $\phi_a(x, y)$ and $\phi_b(x, y)$ are substituted into equation (16), $h(x, y)$ could be calculated and shown in figure 6. For clarity, the one-dimensional height distribution along the dotted line in figure 6 is shown in figure 7, it can be seen that there are five grooves whose heights with respect to the reference point are about −15 μm, −25 μm, −35 μm, −50 μm and −90 μm, respectively.

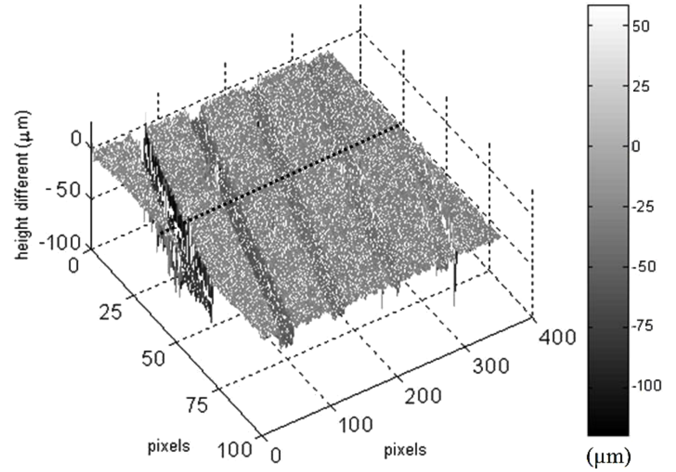

Figure 6. Surface profile of the tested sample with respect to the reference pixel (10, 10).

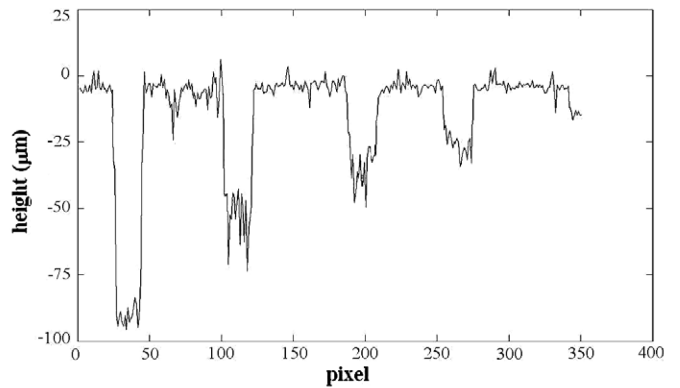

Figure 7. One-dimensional profile along the dotted line in figure 6.

4. Discussion

From equations (6) and (16) we get

$$\delta h_1 = \frac{\partial h}{\partial \phi}\delta\phi + \frac{\partial h}{\partial \lambda}\delta\lambda, \quad (18)$$

and

$$\delta h_2 = \frac{\partial h}{\partial \phi}\delta\phi + \frac{\partial h}{\partial \Lambda}\delta\Lambda, \quad (19)$$

where $\delta\Lambda$ is the error of Λ, and it can be expressed as $\delta\Lambda = (\partial\Lambda/\partial\lambda_a)\,\delta\lambda_a + (\partial\Lambda/\partial\lambda_b)\,\delta\lambda_b$; $\delta\lambda$ is the error of λ; $\delta\phi$ is the error of ϕ_2; δh_1 and δh_2 are the errors of h for smooth regions and discontinuous regions, respectively. The error $\delta\phi$ may be caused by the sampling error $\delta\phi_1$ [20], the polarization mixing error $\delta\phi_2$ [21, 22] and the phase error $\delta\phi_3$ coming from the ambient motion. All the parameters f, f_s, T and g can affect $\delta\phi_1$. $\delta\phi_1$ becomes smaller as T, g and f_s/f increase, and the data processing also becomes time consuming. If Tf is an integer and is larger than 1, the same frame data will be recorded Tf times. Consequently, $\delta\phi_1$ hardly becomes smaller theoretically. To decrease the effect coming from the instability of frequency difference f, we choose the condition

$Tf = 30$ in our tests. Under our experimental conditions, $\delta\phi_1$ can be minimized to 0.036° [20]. The extinction ratio of the AN (Newport Inc.) is 1×10^{-3}; $\delta\phi_2$ can be reduced to 0.027°. According to the specification of our light source, $\delta\lambda_a = \delta\lambda_b \approx 0.02$ nm can be obtained. So, we have $\delta\Lambda = 12.68$ nm. In our practical tests, surrounding vibration and air turbulence affect our measurement results, and their phase errors are up to about $\delta\phi_3 \approx 0.5°$. So, the total experimental phase error $\delta\phi = \delta\phi_1 + \delta\phi_2 + \delta\phi_3 \approx 0.563°$. Consequently, it can be concluded that $\delta h_1 = 0.5$ nm (with $\lambda = 633$ nm) and $\delta h_2 = 0.16$ μm (with $\Lambda = 200.977\,\mu$m). Hence, this method has both merits of the two-wavelength inteferometry and the heterodyne interferometry. In addition, if no reference point is chosen in advance, then the measurement results will be varied according to the optical setup. Although the results are different, the measured profile is similar. To assure good repeatibility of this method, we suggest it is better to choose a convenient reference point on the S in the test.

5. Conclusions

In this paper, an alternative full-field interferometric profilometry has been proposed by combining two-wavelength interferometry and heterodyne interferometry. In this method, heterodyne interferometry is introduced into a modified Twyman–Green interferometer. The full-field heterodyne interference signals are taken by a fast CMOS camera. The associated phase of each pixel can be derived with a least-square sine fitting algorithm. To avoid the phase ambiguity, the two-wavelength technique is used. Finally, the profile of the tested sample can be derived. Its validity has been demonstrated. Hence, this method has merits of both heterodyne interferometry and two-wavelength interferometry such as high resolution, wide measurable range and easy operation.

Acknowledgment

This study was supported in part by the National Science Council, Taiwan, Republic of China, under Contract NSC94-2215-E-009-002.

References

[1] Malacara D 2007 *Optical Shop Testing* 2nd edn (New York: Wiley) chapter 15
[2] Akiba M., Chan K P and Tanno N 2003 Full-field optical coherence tomography by two-dimensional heterodyne detection with a pair of CCD cameras *Opt. Lett.* **28** 816-8
[3] Creath K. 1987 Step height measurement using two-wavelength phase-shifting interferometry *Appl. Opt.* **26** 2810-6
[4] Yokoyama S, Ohnish J, Iwasaki S, Seta K, Matsumoto H and Suzuki N 1999 Real-time and high-resolution absolute-distance measurement using a two-wavelength superheterodyne interferomete *Meas. Sci. Technol.* **10** 1233–9
[5] Wang K and Zeng L. 2005 Two-dimensional surface profile imaging technique based on a double-grating frequency shifter *Appl. Opt.* **44** 4625–30
[6] Schmit J and Hariharan P 2006 Two wavelength interferometric profilometry with a phase-step error-compensating algorithm *Opt. Eng.* **45** 115602
[7] Roy M, Sheppard C J R and Hariharan P 2004 Low-coherence interference microscopy using a ferro-electric liquid crystal phase-modulator *Opt. Exp.* **12** 2512–6
[8] Petr K 2008 A simple interferometric method for determining the flatness of large optical flats with 1 nm repeatability *Meas. Sci. Technol.* **19** 107001
[9] Han H 2008 Achieving traceability and sub-nanometer uncertainty using interferometric techniques *Meas. Sci. Technol.* **19** 084002
[10] Gao F, Leach R K, Petzing J and Coupland J M 2007 Surface measurement errors using commercial scanning white light interferometers *Meas. Sci. Technol.* **19** 015303
[11] Chen L C, Huang Y T, Lai H W, Chen J L and Chang C C 2008 Innovative automatic resonant mode indentification for nano-scale dynamic full-field characterization of MEMS using interferometric fringe analysis *Meas. Sci. Technol.* **19** 125303
[12] Dorrington A A, Cree M J, Payne A D, Conroy R M and Carnegie D A 2007 Achieving sub-millimetre precision with a solid-state full-field heterodyning range imaging camera *Meas. Sci. Technol.* **18** 2809–16
[13] Bitou Y 2005 Two-wavelength phase-shifting interferometry with a superimposed grating displayed on an electrically addressed spatial light modulator *Appl. Opt.* **44** 1577–81
[14] Suzuki T, Yazawa T and Sasaki O 2002 Two-wavelength laser diode interferometer with time-sharing sinusoidal phase modulation *Appl. Opt.* **41** 1972–6
[15] Tkaczyk T and Jozwicki R 2003 Full-field heterodyne interferometer for shape measurememt: experimental characteristics of the system *Opt. Eng.* **42** 2391–9
[16] Pitter M C, See C W and Somekh M G 2004 Full-field heterodyne interference microscope with spatially incoherent illumination *Opt. Lett.* **29** 1200–2
[17] IEEE 2000 IEEE standard for terminology and test methods for analog-to-digital converters *IEEE Std. 1241-2000* 25-9
[18] Farrell C T and Player M A 1994 Phase-step insensitive algorithms for phase-shifting interferometry *Meas. Sci. Technol.* **5** 648–52
[19] Su D C, Chiu M H and Chen C D 1996 Simple two frequency laser *Prec. Eng.* **18** 161–3
[20] Jian Z C, Chen Y L, Hsieh H C, Hsieh P J and Su D C 2007 An optimal condition for the full-field heterodyne interferometry *Opt. Eng.* **46** 115604
[21] Hou W and Wilkening G 1992 Investigation and compensation of the nonlinearity of heterodyne interferometers *Prec. Eng.* **14** 91–8
[22] De Freitas J M and Player M A 1993 Importance of rotational beam alignment in the generation of second harmonic errors in laser heterodyne interferometry *Meas. Sci. Technol.* **4** 1173–6